Macromolecules

ARTICLE

pubs.acs.org/Macromolecules

High-Strain-Induced Deformation Mechanisms in Block−Graft and Multigraft Copolymers

R. Schlegel,[†] Y. X. Duan,[‡] R. Weidisch,[*,†,§] S. Hölzer,[†] K. Schneider,[∥] M. Stamm,[∥] D. Uhrig,[⊥] J. W. Mays,[⊥,#] G. Heinrich,[∥] and N. Hadjichristidis[¶]

[†]Fraunhofer Institute for Mechanics of Materials IWM, D-06120 Halle, Germany

[‡]Key Laboratory of Rubber-Plastics (QUST), Ministry of Education, Qingdao University of Science and Technology, Zhenzhou Road, Qingdao 266042, China

[§]Institute of Chemistry, University of Halle, D-06099 Halle, Germany

[∥]Leibniz-Institut für Polymerforschung Dresden e.V., Hohe Strasse 6, D-01069 Dresden, Germany

[⊥]Center for Nanophase Materials Sciences, Oak Ridge National Laboratory, Oak Ridge, Tennessee 37831, United States

[#]Department of Chemistry, University of Tennessee, Knoxville, Tennessee 37996, United States

[¶]Department of Chemistry, University of Athens, Athens 157 71 Greece, and Life Sciences & Engineering Division, King Abdullah University of Science and Technology (KAUST), Thuwal 23955-6900, Kingdom of Saudi Arabia

ABSTRACT: The molecular orientation behavior and structural changes of morphology at high strains for multigraft and block−graft copolymers based on polystyrene (PS) and polyisoprene (PI) were investigated during uniaxial monotonic loading via FT-IR and synchrotron SAXS. Results from FT-IR revealed specific orientations of PS and PI segments depending on molecular architecture and on the morphology, while structural investigations revealed a typical decrease in long-range order with increasing strain. This decrease was interpreted as strain-induced dissolution of the glassy blocks in the soft matrix, which is assumed to affect an additional enthalpic contribution (strain-induced mixing of polymer chains) and stronger retracting forces of the network chains during elongation. Our interpretation is supported by FT-IR measurements showing similar orientation of rubbery and glassy segments up to high strains. It also points to highly deformable PS domains. By synchrotron SAXS, we observed in the neo-Hookean region an approach of glassy domains, while at higher elongations the intensity of the primary reflection peak was significantly decreasing. The latter clearly verifies the assumption that the glassy chains are pulled out from the domains and are partly mixed in the PI matrix. Results obtained by applying models of rubber elasticity to stress−strain and hysteresis data revealed similar correlations between the softening behavior and molecular and morphological parameters. Further, an influence of the network modality was observed (random grafted branches). For sphere forming multigraft copolymers the domain functionality was found to be less important to achieve improved mechanical properties but rather size and distribution of the domains.

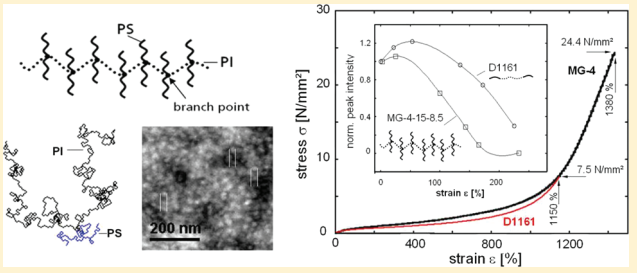

1. INTRODUCTION

Understanding the correlations between new molecular architectures of thermoplastic elastomers and their mechanical properties is of significant importance in polymer science. During the past decades the synthesis techniques of graft copolymer architectures have been successively improved where macromonomers of polystyrene and polyisoprene serve as building blocks from which to create complex model architectures.[1−4] Multigraft and block−graft copolymers are novel types of such macromolecules demonstrating the wide freedom to construct, modify, and tailor such systems. Until now an understanding of how modification of molecular architecture can be used to specifically adjust a certain mechanical property profile has not been achieved. The superelastic nature of these polymers requires further detailed and reasonable explanation. It is important to note that the modification of molecular architecture is not the only means of adjusting the behavior of block copolymer materials. Blending triblock copolymers with a certain amount of diblocks is a common method of reducing the hardness and increasing the strain at break. However, this method strongly reduces the stress at break of these polymers. For triblock−diblock and triblock−diblock−resin blends, investigations on mechanical behavior combined with models of rubber elasticity were carried out by Roos and Creton, showing that the amount of diblocks controls the ratio between entanglements and cross-links.[5] This finding was demonstrated by the observation that for

Received: June 16, 2011
Revised: October 20, 2011
Published: November 10, 2011

the triblocks blended with 60 wt % of a tackifying resin (small molecule with high T_g) the residual strain was similar to that of the pure triblock. For multigraft copolymers the increase of strain at break can be controlled by the molecular architecture, while the preservation of tensile strength is significantly better than triblock−diblock blends. Studies have been carried out considering the cyclic deformation behavior. Additionally, models of rubber elasticity have been applied to softening effects in multigraft copolymers, taking into account filler particles.[6,7] Furthermore, the deformation-dependent molecular orientation of tri- and tetrafunctional multigraft copolymers was studied by in situ FT-IR measurements.[8,9] The aim of the present paper is to investigate the large-scale deformation behavior of block−graft and multigraft copolymers and, by combining the findings from mechanical tests and modeling with information obtained from in situ FT-IR and synchrotron SAXS measurements, to deduce a reasonable explanation for their superelasticity and efficiency of physical cross-linking.

2. EXPERIMENTAL SECTION

2.1. Materials. The molecular architectures of the investigated polymers are shown in Figure 1. Tri- and tretrafunctional multigraft copolymers (Figure 1a,b) consist of a rubbery polyisoprene backbone chain (dotted lines) with grafted PS branches, which are regularly spaced along the backbone. For multigraft copolymers (MG) the nomenclature MG-n-ϕ-β was introduced, where n is the functionality, ϕ is the volume content of PS phase, and β is the number of PS-grafting points. To illustrate the molecular architecture, Figure 2a shows a two-dimensional random walk of a tetrafunctional branch point. Detailed molecular simulations of multigraft copolymers were carried out by Sumpter.[10] Details regarding the anionic synthesis techniques of these graft- and multigraft copolymers can be found elsewhere.[3,4,11] Block−double-graft copolymers (BDG) as shown in Figure 1c are in principle composed of an SIS triblock backbone with PI and PS arms or SI diblocks grafted to the middle or end blocks. In contrast to multigraft copolymers these blocks are grafted randomly. Three types of block−grafts where investigated: (a) PS−PI(I)$_{10}$−PS termed BDG 1. (b) PS(S)$_5$−PI(I)$_{10}$−PS(S)$_5$ termed BDG 4, and (c) PS−PI(SI)$_4$−PS termed BDG 6. Figure 2c shows the outer blocks of the BDG types drawn to scale.

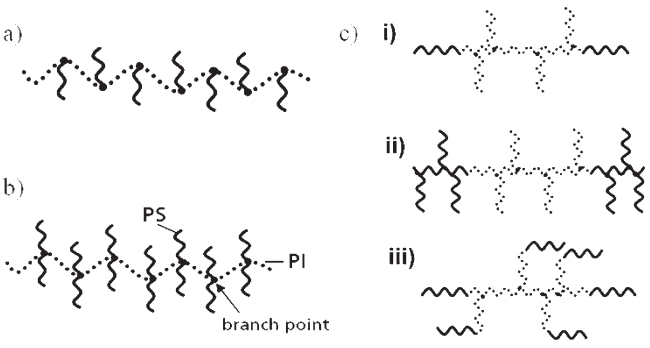

Figure 1. Molecular architecture of (a) trifunctional, (b) tetrafunctional multigraft copolymers,[11] and (c) block−graft copolymers: (i) BDG 1, (ii) BDG 4, (iii) BDG 6.

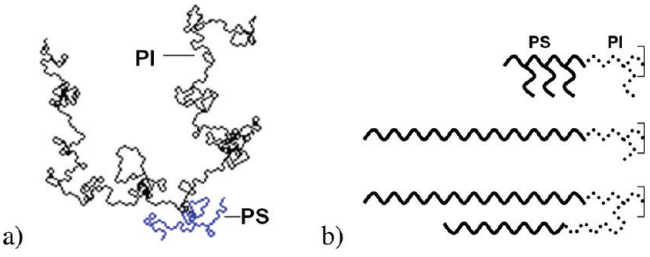

Figure 2. (a) Two-dimensional random walk showing a repeating unit of a tetrafunctional multigraft copolymer. (b) Outer blocks of block−graft copolymers (Figure 1c) drawn to scale.

The molecular weight of the graft copolymers was measured by size exclusion chromatography with multiangle light scattering detection (SEC-MALLS).[3,4] Relevant molecular characteristics are summarized in Table 1, where $M_{w,spacer}$ is the molecular weight between two adjacent PS grafts, $M_{w,graft}$ is the molecular weight of the arms, and $M_{w,block}$ refers to the outer blocks. The overall molecular weight of multigraft chain is obtained by multiplying M_w of a repeating unit with the number of branch points resulting in values between 400 and 980 kg/mol. As a reverence material, the commercially available TPE Kraton D1161 was chosen, which is a SIS−SI triblock−diblock copolymer with about 15 wt % PS and similar to the MG 4 multigrafts. The amount of diblock copolymer is 19 vol %.

2.2. Experimental Methods. Samples were prepared by solution casting. The polymers were dissolved in toluene, and the solutions were poured into glass forms, allowing the solvent to evaporate over 7 days. To remove residual toluene, the polymer films were annealed at 70 °C under vacuum for 3 days. For mechanical testing, dog-bone samples according ISO 527-2 of type 5B (overall length 20 mm, parallel length 6 mm) were stamped from the films. Mechanical characterization was performed with a Zwick/Roell universal testing machine Z020 equipped with a 500 N load cell. The samples were deformed at a constant strain rate of 0.025 s^{-1} cross-head displacement, resulting in a true strain rate of 0.0204 ± 1.3 × 10^{-3} s^{-1}. The strain was measured by an optical method using an imaging system (GOM, Aramis). Images were taken at a constant time interval, and the positions of the markers were automatically detected based on the gray scale value profile (Figure 3). The obtained optical true strain was further correlated to the stress data at equal time intervals and plotted in σ vs ε diagrams to apply the rubber elasticity models.

The morphology was characterized by synchrotron SAXS at DESY Hamburg (BW4 at DORIS III storage ring). Scattering patterns were obtained at a sample to detector distance of typically 6049 mm. The wavelength of characteristic radiation was 0.138 nm. The samples were mounted in a modified mechanical testing device (Kamrath and Weiss) which was additionally used to measure strain-dependent scattering patterns.[12] The average domain distance d_{av} was calculated according to

Table 1. Molecular Data of Multigraft and Block−Graft Copolymers

	Φ_{PS} [vol %]	$M_{w,PI\text{-}spacer}$ [kg/mol]	$M_{w,PS\text{-}graft}$ [kg/mol]	$M_{w,PI\text{-}graft}$ [kg/mol]	$M_{w,PS\text{-}block}$ [kg/mol]	M_w [kg/mol]
MG-3-17-β	17	86	32			β·117
MG-4-15-β	15	97	11			β·104
BDG 1	28	73		2.4	21.5	145
BDG 4	28	68	2.7	3.3	7.7	143
BDG 6	30	163 (backbone) 41 (average)	12 (PI−PS grafts)		21.5	287

dx.doi.org/10.1021/ma201353w |Macromolecules 2011, 44, 9374–9383

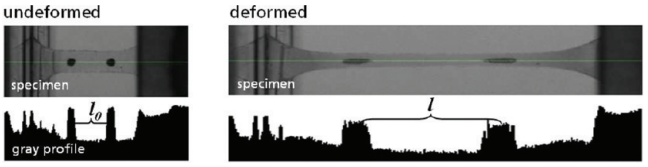

Figure 3. Undeformed and deformed elastomer samples with optical markers and corresponding gray profile (l_0: distance at $t = 0$ s; l: marker distance during deformation).

the relation $d_{av} = 2\pi/q^*$, where q^* is the position of the primary reflection peak.

FT-IR measurements were carried out in the group of Prof. H. W. Siesler at University Essen using a Bruker IFS88FT-IR spectrometer with a spectral resolution of 4 cm^{-1}. The samples were stretched with an electromechanical film stretching device mounted in the sample compartment of the spectrometer. About 30−40 μm thick films were deformed at a constant rate of 3.2 mm/min. The polarization direction of the IR radiation was adjusted by a pneumatically rotatable wire-grid polarizer (SPECAC) to obtain the spectra parallel and perpendicular to the stretching direction by a rapid 90° rotation.[9]

2.3. Applied Models. Stress−strain data were analyzed by applying the slip-tube model of Rubinstein and Panuykov.[13] The stress response is described by eq 1, where $G_{c,ST}$ and $G_{e,ST}$ are the chemical and the physical cross-link modulus and λ is the elongation ratio l/l_0.

$$\sigma^{load} = \left(\lambda - \frac{1}{\lambda^2}\right)\left(G_{c,ST} + \frac{G_{e,ST}}{0.74\lambda + 0.61\lambda^{-0.5} - 0.34}\right) \quad (1)$$

In contrast to more complex models including strain hardening effects, the parameters of the slip tube model are easy to obtain by plotting the reduced stress $\sigma_R = \sigma^{load}/(\lambda - \lambda^{-2})$ vs the expression $(0.74\lambda + 0.61\lambda^{-0.5} - 0.34)^{-1}$. By this procedure, eq 1 reduces to an equation of the type $y(x) = a + bx$, where a and b are the two moduli. In contrast, in the case of the nonaffine tube model taking into account finite chain extensibility, a nonlinear least-squares algorithm with several iteration cycles is required to fit the data. However, the advantage of the latter model is that it covers all experimental data and therefore offers a better accuracy in the obtained model parameters. This model yields additionally a parameter representing the portion of elastically active entanglements (n), which is defined by n_e/T_e, where T_e is the Langley trapping factor. This parameter can be understood as the probability that a certain entanglement becomes a permanently trapped one and n_e as the number of statistical chain segments between two successively trapped entanglements.[14] T_e was assumed as unity for all investigated polymers. However, based on sol extraction measurements, the value can be calculated for chemical cross-linked networks.[15] The stress response during uniaxial loading is obtained by deriving the strain energy function of the model with respect to the elongation λ, resulting in eq 2.

$$\sigma_0^{load} = G_c\left(\lambda - \frac{1}{\lambda^2}\right)\left(\frac{1-\frac{1}{n}}{\left(1-\frac{1}{n}\left(\lambda^2 + \frac{2}{\lambda} - 3\right)\right)^2} - \frac{\frac{1}{n}}{1-\frac{1}{n}\left(\lambda^2 + \frac{2}{\lambda} - 3\right)}\right) + 2G_e\left(\frac{1}{\sqrt{\lambda}} - \frac{1}{\lambda^2}\right) \quad (2)$$

Load cycles of hysteresis curves were evaluated using this extended nonaffine tube model of rubber elasticity with finite chain extensibility according to eq 2.[16,17] The parameters G_c and G_e of the slip tube are comparable with nonaffine tube if the model fit is performed below the inflection point of the stress−strain curve. Finite chain extensibility results the up turn of the stress−strain curve at high strains. This was especially observed for predeformed samples where in contrast to undeformed samples the inflection point is shifted to lower values.

Further, the hysteresis unload curve was characterized by applying an energy-based softening model in eq 3, where $W(\lambda)$ and W_{max} are the strain energy functions of the nonaffine tube model during deformation and at maximum elongation, respectively, b is a softening parameter, and σ_0^{load} is the stress response of the initial load curve.[18]

$$\sigma^{unload} = \sigma_0^{load}\exp(-b\sqrt{W_{max} - W(\lambda)}) \quad (3)$$

Table 2. Morphology and Average Domain Distance d_{av}

material	morphology	d_{av} [nm]
MG-3-17-3.7	spherical	40
MG-4-15-5.1	spherical	25
MG-4-15-8.5	spherical	23
BDG 1	cylindrical	37
BDG 4	cylindrical	39
BDG 6	lamellae (weakly ordered)	29

3. RESULTS AND DISCUSSION

3.1. Molecular Deformation Behavior and Morphological Aspects. Morphology and average domain distance d_{av} of the undeformed polymers are shown in Table 2. The tri- and tetrafunctional multigrafts form spherical PS domains. It is known from other block copolymer morphology work that these domains can be arranged in a face-centered cubic (fcc), body-centered cubic (bcc), and hexagonal close-packed (hcp) lattice structure.[19,20] In the presents studies no long-range order was observed for sphere forming multigrafts. The average domain distance d_{av} is clearly decreasing with increasing functionality and slightly decreasing with the number of branch points. Multigraft copolymer morphology can be predicted by combined use of the Milner phase diagram and the constitutive block copolymer concept, which is in fair agreement with the observed morphologies.[21−23]

For the block−graft copolymers BDG 1 and BDG 4, d_{av} was observed to be governed by $M_{w,PI\text{-}spacer}$ and further by the number and lengths of the PI arms grafted to the middle block. The former aspect is reasonable because the end-to-end distance r is increasing by higher M_w. Further the same effect is obtained by increasing M_w of the grafted side chains, which can be expected to expand the polymer coil of the backbone. BDG 6 exhibited a weakly ordered lamellar morphology, as supported both by a peak at $2q^*$ in the scattering diagram and by a slight yield point during tensile testing; however, TEM micrographs could not clearly verify this order.

To correlate molecular data with the results of microstructural investigations, the number of PS arms necessary to form one domain (functionality of domains) should be obtained, which is of importance to discuss the efficiency of physical cross-linking. As a first approximation the average PS domain size should be calculated from the known value of the PS content and the average domain distance. The assumption of densely filled phases (PS and PI) is strictly not true; however, results are in fair agreement with experimental data as shown later. The volume of the spherical PS domains can be estimated by eq 4, where $d_{av,PS}$ is the diameter of the PS sphere, $d_{av,PI-PS}$ is the average PI−PS domain distance, and Φ_{PS} is the volume fraction of PS. Assuming

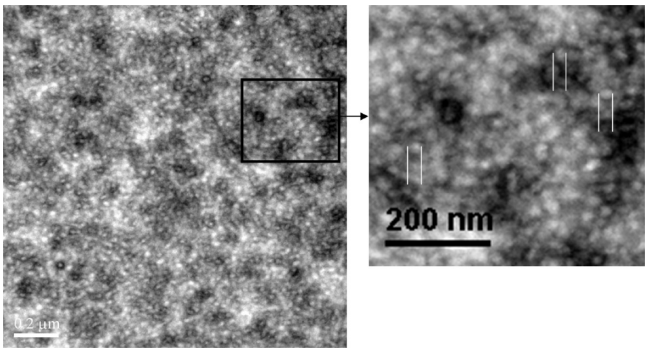

Figure 4. TEM micrograph of the morphology of MG-3-17-3.7.

a bcc order, $d_{av,PS,sph}$ can be obtained with the relation given in eq 5. The number of PS monomers per sphere is obtained by eq 6, where $V_{s,seg}$ is the segmental volume of styrene (0.176 nm^3).[23] This value is slightly different form that calculated by the relation $V_{PS,seg} = M_{w,PS\text{-}mon}/(\rho N_{Av})$, with $M_{w,PS\text{-}mon}$ the molecular weight of PS monomer, ρ the density of PS, and N_{Av} the Avogadro number, which equals 0.19 nm^3. Finally, the number of PS grafts forming one domain is obtained by eq 7, where $N_{PS,arm}$ is the degree of polymerization of one graft.

$$V_{PS,sph} = \frac{1}{6}\pi {d_{av,PS}}^3 \tag{4}$$

$$V_{bcc} = \Phi_{PS} = \frac{2V_{sph}}{V_{lattice}} = \frac{\frac{1}{3}\pi {d_{av,PS,sph}}^3}{{d_{av,PI-PS}}^3};$$

$$d_{av,PS,sph} = d_{av,PI-PS}\sqrt[3]{\frac{3}{\pi}\Phi_{PS}} \tag{5}$$

$$N_{PS,sph} = V_{PS,sph}/V_{PS,seg} \tag{6}$$

$$n_{PS,grafts} = N_{PS,sph}/N_{PS,arm} \tag{7}$$

Thus, with MG-3-17 showing a $d_{av,PI-PS}$ of ~40 nm and MG-4-15 of about 25 nm, we can calculate the average values for $d_{av,PS,sph}$ of 24 and 14.5 nm, respectively. For the trifunctional multigraft this is in accordance with TEM micrographs shown in Figure 4, where the average diameter of the PS domains is in between 23 and 27 nm. Further, the functionalities of the PS spheres (number of branch points connected to the domains) according eq 7 are 128 and 40 for tri- and tetrafunctional MGs, respectively.

On the basis of computer simulations, Sumpter has shown that the PS arms of tetrafunctional branch points form pseudo-spherical domains with several intradomain interactions of the PS grafts.[11] These small domains were further suggested to interact (interdomain interactions) with other domains forming larger clusters.

Now these findings should be correlated to the orientation of PI and PS monomers during deformation by results from FTIR, which can be used to obtain information on the efficiency of physical cross-linking in dependence of the number of grafting points. The orientation functions of both PS and PI monomers are plotted in Figure 5 vs the applied strain. In Figure 5, f is the orientation function perpendicular to the stretching direction (SD) calculated by the relation $f = -2(R - 1)/(R + 2)$. R represents the dichroic ratio given by $R = A_{\parallel}/A_{\perp}$, with $A_{\parallel}$ and $A_{\perp}$ being the absorbencies of the selected IR band parallel and perpendicular to SD, respectively. The method of data analysis can be found in our former publications.[8,9]

The orientation function was observed to show an increasing trend with higher strain for tetrafunctional multigraft copolymers and also for trifunctional MGs (not shown). This increase indicates that the domains are deformable up to high external strains. $\Delta f_{PI,PS}$ represents the difference in the orientation functions of PI and PS. Between 1300 and 1400% strain, this value was found to be about 0.05 for a trifunctional architecture with 2.6 branch points (larger domains as compared to MG-4-15), while it was ~0.01 for the MG-4-15-5.1 (Figure 5a). The difference appears reasonable when comparing the average diameter of the PS spheres. These finding suggest lower interfacial area and a larger amount of unoriented PS monomers in the cores of the domains for the MG-3-17 type. The ratio of orientable to unorientable PS monomers can be assumed to be higher for the tetrafunctional MG, which is reflected in the reduced value of $\Delta f_{PI,PS}$. For the tetrafunctional MG with lower number of branch points (Figure 5b) larger differences between the orientation functions were observed, although the average domain distances (23−25 nm) are similar to MG-4-15-5.1.[24] In the case of MG-4-15-3.3 (Figure 5b) $\Delta f_{PI,PS}$ first becomes obvious at about 600%, where f_{PS} reaches a plateau. However, such a plateau was not observed for the MG-3-17 material.[8] This effect may be attributed to the physical cross-linking density expressed by the number of I_2S_2 repeating units (β). Obviously, multigrafts with high β and small domains can keep the cohesion of the domains at high strains because the internal stress is distributed to a larger number of grafting points and therefore spherical domains. This assumption is reasonable because for spherical morphologies it was shown that domain−domain bridging is the most probable configuration of the PI spacer.[8,25] For the appearance of the plateau, two explanations may be given: (a) PS grafts are pulled out of the domains if a critical stress is achieved, and they return to its original coiled configuration; (b) a fracture of PS domains without further orientation of the monomers.

Because of the confinement by neighboring PI chains which prevent a return of the PS grafts to their coiled shape, point (a) appears to be unreasonable. Therefore, is must be concluded that the continuous orientation of PS covers both effects chain pull out and orientation of PS monomers in the interface. The partial or complete pullout of PS grafts we term stress-induced mixing of polymer chains. The fact that in case of the MG-3-17 material no plateau was observed (obviously no fracture of the domains) may be attributed to the larger M_w of the grafts, which on the one hand results in a stronger PS−PS interaction; on the other hand, this distributes the stress to a reduced number of domains. The decrease of T_g by reduction of graft M_w is less important because this would only reduce the glass transition temperature of PS to about 360 K.[26] Additionally, less attention must be paid to the entanglement M_w of PS[26,27] because testing temperature is far below the $T_{g,PS}$.

3.2. Deformation Characteristics. The tensile and hysteresis behavior of multigraft and block−graft copolymers are now discussed. The mechanical data were analyzed by the slip tube

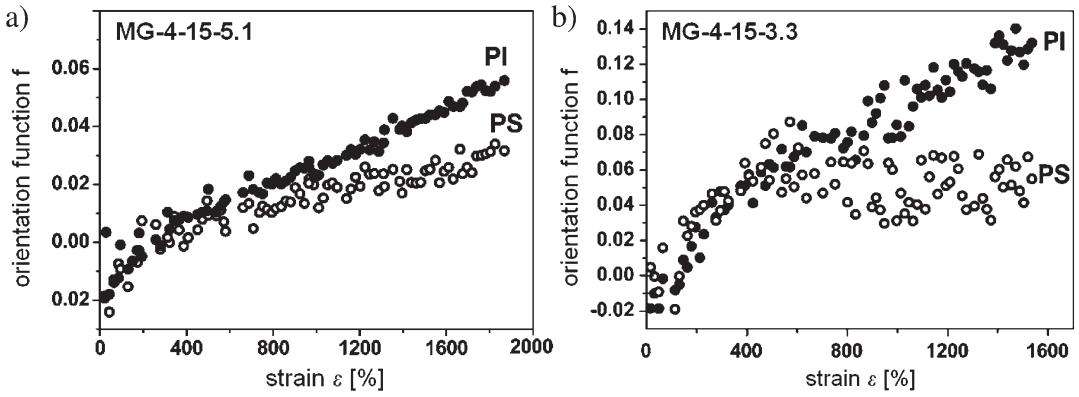

Figure 5. Strain-dependent orientation function of tetrafunctional multigraft copolymers.[9]

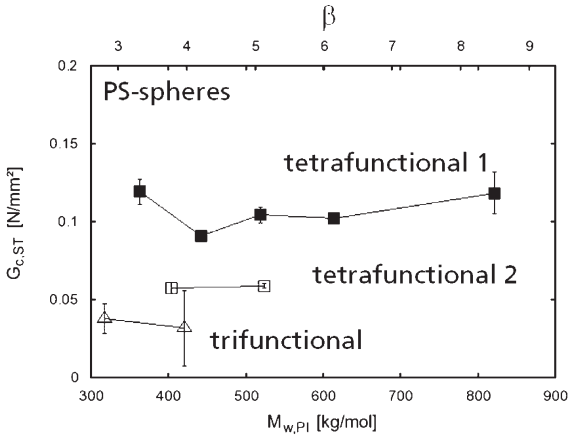

Figure 6. Chemical cross-link modulus obtained from the slip tube model for tri- and tetrafunctional multigraft copolymers with 15−17 vol % PS (tetrafunctional 1 and 2 are multigrafts of type MG-4-15 originating from different batches).

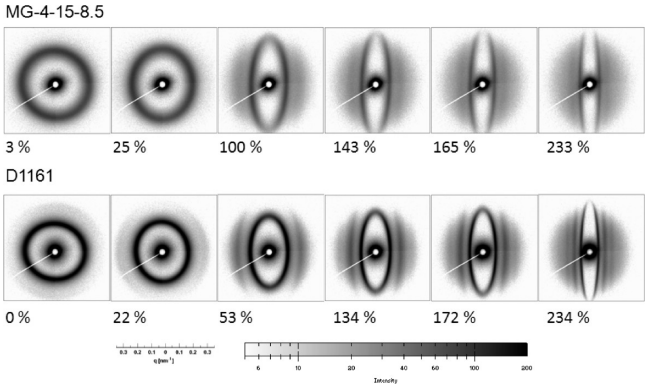

Figure 7. Scattering pattern of the sphere forming tetrafunctional multigraft copolymer and Kraton D1161, stretching direction horizontally.

and the nonaffine tube model. Investigations on the fractured morphology of block−graft copolymers are also presented.

3.2.1. Tensile Behavior of Sphere Forming Multigraft Copolymers. The deformation behavior of multigrafts with spherical morphology was characterized through medium elongations below the inflection point of the stress−strain curve by applying the slip tube model to the tensile data, and the chemical $G_{c,ST}$ and physical $G_{e,ST}$ cross-link modulus were obtained. $G_{c,ST}$ is plotted vs the molecular weight of the PI backbone and the number of branch points β in Figure 6. In contrast to the G_e, which was found to increase slightly with β,[28] $G_{c,ST}$ is independent of the overall molecular weight. This observation is reasonable because the investigated multigrafts are regularly spaced. The slight increase of $G_{c,ST}$ above 4 branch points (tetrafunctional 1) may be attributed to the improved distribution of the PS domains in the matrix. G_c is nearly branch point independent for tetrafunctional multigrafts. Such constancy may be understood because this value is obtained at medium elongations below 500% where the stress acting on each branch point is low (see section 3.1).

The in situ deformation characteristics were studied by synchrotron SAXS. Figure 7 shows the in situ deformation scattering pattern of the tetrafunctional multigraft copolymer MG-4-15-8.5 and Kraton D1161. Because the average domain distance decreases with increasing ring radius of the primary reflection peak, D1161 shows a lower value for d_{av} (29 nm) in comparison to MG-4-15-8.5 (22.4 nm). The patterns become elliptical by increasing the deformation. d_{av} increases in the stretching direction while it decreases perpendicular to it.

For Kraton D1161 a secondary and ternary reflection peak can be observed. The ratio between the position of the secondary and primary peak reflection is at about $1.73q^*$ at medium to high elongations. This value was also observed for the tetrafunctional multigraft copolymer, while the intensity of the secondary reflection peak is obviously less. The formation of an ordered structure may be caused by finite extensibility of the PI chains. Short chains can be assumed to reach their finite extensibility earlier than long chains, and the stress is forcing the spherical domains into an ordered structure. This tendency is more pronounced for the D1161 in comparison to MG-4-15 architecture. From literature three types of densely packed structures are known (fcc, bcc, hcp).[20] The scattering positions at $1.74q^*$ is correlating to the (110) reflection in the hcp structure. Further, for the stretched Kraton D1161 a peak at about $2.5q^*$ appears, which may correspond to the (203) diffraction plane of hcp (Figure 8). Other peaks cannot be found. It can be assumed that by stretching these polymers the domains are forced into a hcp lattice structure. These domains are at about 11.7 nm in diameter for MG-4-15-8.5, while for D1161 $d_{av,PS,sph}$ is 16.5 nm. The fact that nearly no secondary reflection peak is observed illustrates

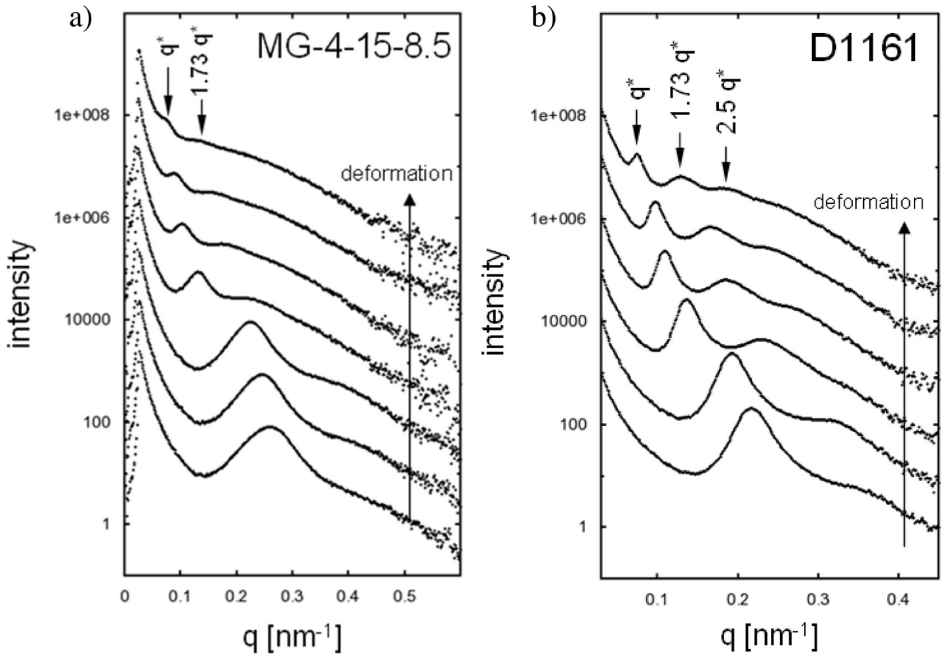

Figure 8. Intensity vs q plot of the scattering pattern in Figure 7 obtained in the stretching direction for (a) MG-4-15-8.5 and (b) Kraton D1161.

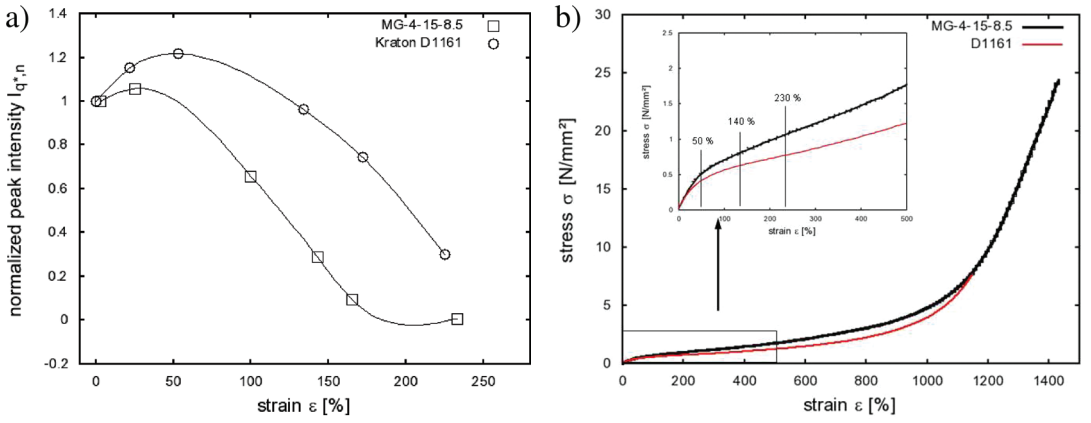

Figure 9. (a) Normalized intensity of the primary reflection peak vs elongation (in stretching direction). (b) Corresponding stress−strain curve of MG-4-15-8.5 and Kraton D1161 (elongation measurement with a Zwick/Roell multiXtens system).

that these domains are highly deformable and that their shape is more maintained in the case of Kraton D1161 (larger domains).

Comparing the undeformed state of the tetrafunctional multigraft copolymer in Figure 7, it becomes obvious that (a) the peak width appears broader and (b) the intensity of the primary reflection peak is less in comparison to Kraton D1161. From this observation it can be concluded that the matrix of the latter contains more effective scattering centers and that the MG-4 copolymer reveals a broader domain size distribution. In Figure 9a, the peak intensity of the primary reflection peak is related to the unstretched state and plotted vs the applied elongation. The peak intensity was obtained by subtracting the intensity at the right bottom of the peak from the intensity at q^*. The scattering intensity of both materials was found to differ clearly. I_{q^*} is about 2−3 times higher for Kraton D1161 in comparison to MG-4. It shows a maximum at about 140% and decreases to round 2 at about 233% strain.

In Figure 8, up to about 50% strain an increase of $I_{q^*,n}$ can be observed, which correlates to the formation of a strain-induced domain ordering. The domains are initially well separated in the undeformed state, and the increase of domain order let assume that the domains approach each other. The inflection point of both curves corresponds to the end of the neo-Hookean region (Figure 9b). For Kraton D1161 the transition to the linear stress−strain region is observed at higher strains in comparison to the MG-4 type (Figure 9b), and the inflection point is shifted in the same direction. Further, elongation results in a reduction of the normalized peak intensity.

This reduction indicates to a decrease of scattering centers in the matrix while the domain order is still increasing. This can be clearly observed by the presents of secondary and primary reflection peaks in Figures 7 and 8. During elongation the embedded PS domains (coiled PS branches) are dissolved in the PI matrix (elongated) by deformation, which was also found

dx.doi.org/10.1021/ma201353w |*Macromolecules* 2011, 44, 9374–9383

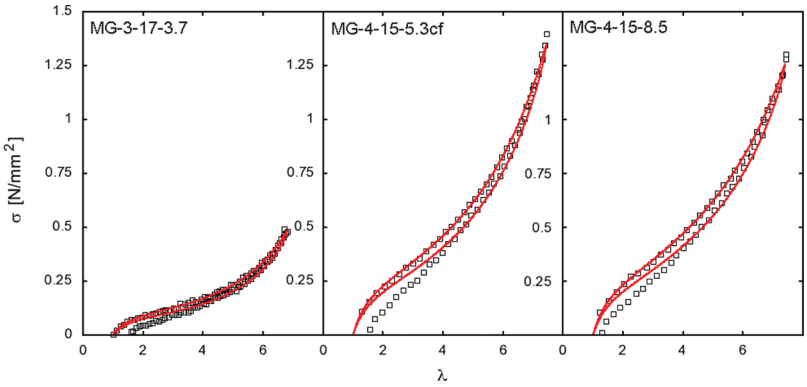

Figure 10. Hysteresis data (squares) and model curves according eqs 2 and 3 (red lines) for tri- and tetrafunctional multigraft copolymers.

Table 3. Model Parameters of the Nonaffine Tube Model with Finite Chain Extensibility and the Softening Model

	nonaffine tube model			
	G_c [kPa]	G_e [kPa]	n	softening model b (N m)$^{-1/2}$
MG-3-17-3.7	26	48	114	0.177
MG-4-15-5.3cf	84	86	171	0.086
MG-4-15-8.5	90	80	197	0.083
BDG 4	48	95	113	0.13
BDG 1	68	125	109	0.094
BDG 6	296	447	74	0.078

by FT-IR. We assume that this behavior corresponds to a strain induced mixing of the copolymer chains. The polymer chains are assumed to slide along each other, yielding a reduction of the T_g which may promote further sliding.

3.2.2. Cyclic Deformation of Sphere Forming Multigraft Copolymers. Mechanical characterization at high strains was done by performing hysteresis tests of pre-deformed samples and applying the nonaffine tube model to the stress−strain data. The samples were stretched in a first cycle to 900% to pre-deform the morphology and in the second cycle to 700% only to avoid further stress softening. The rubber elasticity model was applied to the second hysteresis cycle because in this cycle softening effects originating from the virgin morphology are less. Hysteresis data and corresponding model curves are shown in Figure 10. The experimental error of the strain measurement method is about 0.5 px, which corresponds here to ∼50 μm. However, this error is less significant because of the high strains. In further work theoretical accuracy of the strain measurement procedure was improved to typically 0.0045 px. A detailed discussion of this development will be part of a future publication. To determine analytical errors, three hysteresis tests of Kraton D1161 samples were performed. The data were evaluated by the nonaffine tube and the softening model. We obtained model parameters and errors for the second cycle at 700% as follows: G_c = 0.136 (±4.2%) MPa; G_e = 0.218 (±1%) MPa, n = 240 (±9.5%), and b = 0.0303 (±15%) (N m)$^{-1/2}$. Because of the limited amount of multigraft and block−graft copolymers, each molecular architecture of these polymers was characterized using only one sample.

In Figure 10, it can be observed that the model curve approaches the point of zero deformation while the experimental data do not. An explanation may be given by the fact that viscoelastic material effects are neglected in the softening model.[18] However, the advantage of this combined model is that it offers a minimum set of parameters which are easily correlated to the material behavior. A closing of the hysteresis curve can be observed if the samples shape enables a tensile and compressive deformation (dumbbells). The presently used dog-bone-shaped samples were exclusively deformed in tensile mode (positive forces).

Pronounced low stress values can be observed for the trifunctional multigraft copolymer with an average domain distance of about 40 nm. The tetrafunctional types with 8.5 and 5.3 (cf = coarsely fractionated) are showing a steeper slope in the middle part, which corresponds to an increase in G_c. All model parameters are summarized in Table 3. The increase of G_c directly correlates with a reduction of the softening parameter. The decrease of b indicates that the unload cycle approaches the load cycle. This correlates with an increase of the PS-domain distribution. By comparing G_c and b for the MG-3 and MG-4 type, it can be concluded that high deformable PS domains are more important to achieve improved mechanical properties than a high functionality of these domains. The model parameter n directly correlates to the molecular weight of the PI spacer. The lower n value of MG-3-17 in comparison to MG-4-15 is in agreement with the molecular weight of the PI backbone chain, which are 86 and 97 kg/mol, respectively. However, it can be observed that the magnitude of the change in n is less reasonable. This parameter almost doubles but $M_{w,PI\text{-}spacer}$ increases by about 13% only. By comparing G_c of the nonaffine tube and the slip tube model, slightly improved values can be observed for the latter model since in case of slip tube the PS domains were considered as filler particles using the Einstein/Guth relation as a prefactor:

$$G_{c,ST} = G^0_{c,ST}(1 + 2.5\Phi_{PS} + 14.1\Phi_{PS}^2) \quad (8)$$

However, multiplying the G_c value of the nonaffine tube with the term in parentheses of eq 8 leads to slightly higher values as obtained by the slip tube model (Figure 6). This difference may be attributed to softening effects from the first to the second cycle. G_c was observed to decrease by about 17−22% between these two cycles. These softening effects can be attributed to two mechanisms: the breakdown of aggregated clusters of spherical domains and also to domain chain pullout (resolving of "physical" cross-links) and fracture of domains. Because of the breakdown of filler cluster aggregates, the estimated modulus $G_{c,ST}$ is expected to be lower for virgin undeformed samples in

dx.doi.org/10.1021/ma201353w |*Macromolecules* 2011, 44, 9374–9383

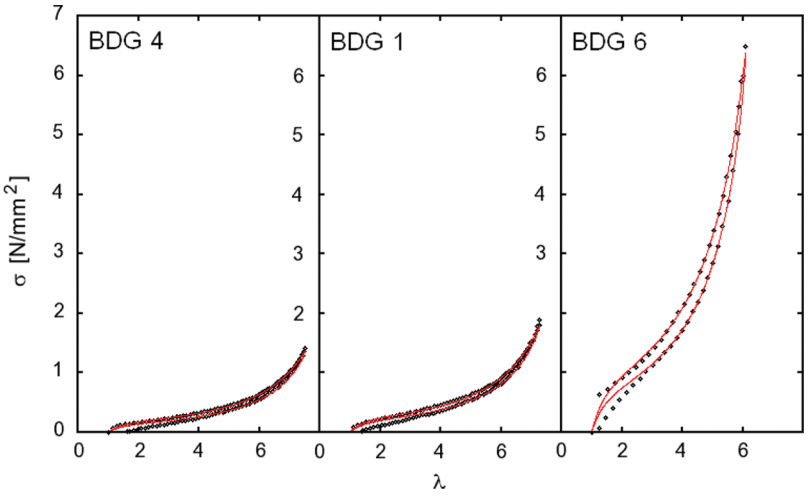

Figure 11. Hysteresis data and model curves for block−double-graft copolymers.

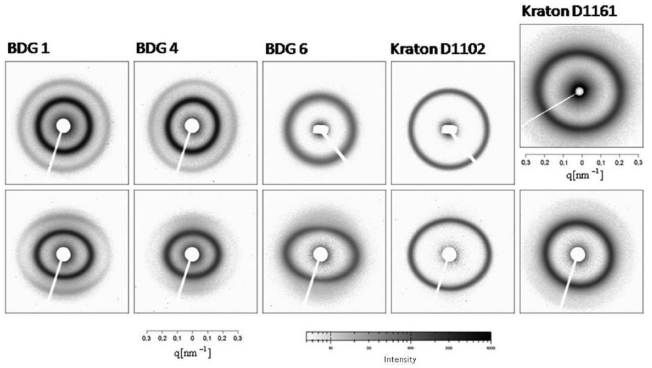

Figure 12. Scattering pattern of block−double-graft and commercially available triblock copolymers: top, undeformed; bottom, after deformation and relaxation (previous stretching direction vertically).

comparison to the modulus G_c from the nonaffine tube model in the second cycle. This assumption is verified when considering $G_{c,ST}$ for MG-3-17-3.7 and MG-4-15-8.5 divided by the Einstein/Guth prefactor.

3.2.3. Cyclic Deformation of Block−Graft Copolymers. Hysteresis and model curves for block−graft copolymers are shown in Figure 11. At similar hysteresis strain the stress response is different for the investigated materials. It is increasing with decreasing d_{av}. In comparison to BDG 1 and 4, a reduced maximum true hysteresis strain can be observed for BDG 6, but the maximum hysteresis stress is exceeding that of BDG 1 and 4 by about a factor of 3.5. The parameters of the nonaffine tube model and the softening model are summarized in Table 3. On the basis of the information from molecular architecture, it can be expected that G_c is decreasing with increasing molecular weight of PS backbone, which is not verified by the comparison between BDG 4 and BDG 1 (Tables 1 and 3). In contrast, BDG 6 reveals an improved G_c, which indicates that not the molecular weight of the PS backbone is important but rather the average $M_{w,PI}$ between neighboring PS blocks, which is about 41 kg/mol. Additionally, significant differences in the mechanical behavior of block−grafts were observed when comparing the model parameters between first and second hysteresis cycle, where G_c reduces by about 72 and 80% for BDG 1 and 4 and by about 30% for BDG 6 only. Aspects contributing to the increase of G_c from BDG 1 to BDG 6 are (i) the reduced d_{av} resulting in a well-dispersed filler structure, (ii) the long PS outer blocks providing an effective connection to the PS domains, and (iii) the small $M_{w,PI\text{-spacer}}$ which increases the chemical cross-link modulus. Contributing further to improved G_c values is the fact that in case of BDG 6 the PS blocks are grafted randomly to the PI backbone, resulting in a multimodal PI network, which is in contrast to MG-3 and MG-4 where PS blocks are in equal distance. Mark has shown that for end-linked PDMS networks strain at break and tensile strength increases by combining small and long network chains.[29] The expectation that strain at break is reduced by small chains (weakest link theory) was not observed because the deformation is highly nonaffine. However, detailed investigations are available only for bimodal networks due to the large molecular combinations for three and more chain lengths. In the case of BDG 4 the PS outer blocks can be considered as branched, and about 10 kg/mol is an estimated value for the average block length. For BDG 1 the M_w of the outer block length is 23.5 kg/mol and for BDG 6 two values 12 kg/mol for the diblock and 21.5 for the triblock have to be taken into account. Under these considerations BDG 6 fulfills the three aspects mentioned before to achieve small well-distributed domains and effective physical cross-linking. The number of statistical segments n as a model parameter most reasonably explains the correlation to $M_{w,PI\text{-spacer}}$. In the case of BDG 6, this value is the lowest among the block−double grafts. The differences between BDG 1 and 4 should be statistically verified by further investigations.

3.2.4. Microstructure of Undeformed and Deformed BDG Types. Deformation characteristics of fractured morphologies of the block−graft types were studies by synchrotron SAXS. Scattering patterns are shown in Figure 12. The patterns reveal at least one primary peak and in the cases of BDG 4 and 1 a secondary reflection peak. The position corresponds to a morphology composed of hexagonally packed cylinders with reflection peaks at $3^{1/2}\ q^*$ and $7^{1/2}\ q^*$. In the case of BDG 6 a slight secondary peak was found at $2q^*$, indicating a lamellar morphology with weak long-range order.

Further, samples of the investigated polymer films were deformed to 800% cross-head displacement and subsequently unloaded to zero force. The samples were removed from the

Table 4. Average Domain Distance of Deformed Samples after about 2 weeks of Relaxation

	BDG 1	BDG 4	BDG 6	D1102	D1161
$d_{av,res,\parallel}$ [nm]	41.6	42.7	36.3	27.8	30.1
$\lambda_{res,\parallel}$	1.09	1.1	1.23	1.1	1.01

clamps, relaxed for about 14 days at room temperature, and again investigated by SAXS. The obtained scattering patterns are shown at the bottom of Figure 12. The elliptical shape of the pattern becomes more pronounced from BDG 4 to BDG 1 to BDG 6. The secondary peak at $(3q)^{1/2*}$ was still observed for the two BDG 4 and BDG 1 architectures. The position of the primary reflection peak is decreasing in the direction in which the sample was originally elongated, and it is increasing perpendicular to it, which corresponds to the average domain distance. d_{av} increases in the stretching direction, and it decreases perpendicular to it. d_{av} was obtained for undeformed and deformed/relaxed samples parallel to the previous stretching direction. These values are summarized in Table 4. Additionally, the triblock copolymer Kraton D1102 (SBS type, 28 wt % PS, 17 wt % diblock) with a cylindrical morphology was investigated for comparison. The residual deformation $\lambda_{res,\parallel}$ was calculated based on the average domain distance of the undeformed samples.

When considering the values of $\lambda_{res,\parallel}$ for the copolymers with cylindrical morphology BDG 1, BDG 4, and Kraton D1102, we can observe similar values. For the disordered morphology of BDG 6 with a weak lamellar long-range order, a clearly higher value of $\lambda_{res,\parallel}$ can be found. In contrast, for Kraton D1161 (spherical PS domains) $\lambda_{res,\parallel}$ is almost identical to the undeformed samples. It is assumed that these parameters are specific for the type of morphology.

Furthermore, when calculating the residual elongation perpendicular to the stretching direction, it was found that the incompressibility condition was not fulfilled. The highest deviation was observed for BDG 6 (+16.5%) while BDG 4 (+14.1%) and D1102 (+15.7%) are similar but slightly below BDG 6. BDG 1 and D1161 were found to show a deviation from incompressibility of +5.3 and +7.2%. It was originally assumed that rigid domain fragments of formally continuous morphologies (BDG 6) are acting as steric hindrances in the back cycle, which do not allow the polymer matrix to return to its original constitution resulting in cavities on nanoscale. However, this assumption could not be verified because the expected additional scattering was not observed. We rather suspect that the polymer matrix keeps a strain induced orientation, which can be interpreted as partial mixing of the polymer chains.

To verify this assumption, the invariant Q was calculated using eq 9 where $I(q_x,q_y)$ represents the scattering intensity and $I_b(q_x,q_y)$ the scattering intensity of the background. q_x and q_y are q components perpendicular and parallel to the stretching direction. The patterns were first harmonized. In a next step every intensity value was multiplied by its distance to the meridian, and finally integration between 90° and 180° was carried out. By a second integration over all available data points of the so-received Iq^2 vs q plot the invariant Q was obtained. This value corresponds to the phase ratio ν and the density contrast $\rho_1 - \rho_2$ in eq 10.

$$Q = \int_0^\infty \int_0^\infty (I(q_x, q_y) - I_b(q_x, q_y))q_x \, dq_y \, dq_x \quad (9)$$

$$Q = (\rho_1 - \rho_2)v(1 - v) \quad (10)$$

For BDG 1 Q was observed to reduce from about 0.0366 to 0.0216 and for BDG 4 from 0.0301 to 0.0181, which is a decrease of about 40−41%. Because the phase ratio ν in eq 10 can be considered as constant, the reduction of Q is originating from a change in density contrast and therefore points to a strain induced mixing of the block copolymer phases.[30]

In contrast to homopolymers, this mixing results in an additional enthalpic contribution and in a retracting force because the mixed phases tend to phase separate again. By this mechanism the T_g of the hard phase can be expected to decrease, which supports further sliding of the different polymer chain types. The strain induced mixing of both PI and PS blocks would explain at least two aspects: (i) the reduction of the peak intensity and constant scattering at small q values and (ii) the reduced contrast in TEM as observed in our other publications.[9] A final conclusion if the deviation from incompressibility condition reflects a strain-induced volume increase on molecular scale or not requires further studies. Thereby, strain calorimetry and positron annihilation lifetime spectroscopy could serve as useful techniques.[31,32]

4. CONCLUSIONS

This work has focused on the molecular and morphological processes taking place during uniaxial monotonic loading of multigraft and block−graft copolymers based on polystyrene and polyisoprene. For sphere forming multigrafts the nearly identical orientation of PS and PI up to high strains and the simultaneous decrease of scattering intensity reveal elongation and partial chain pull out of glassy blocks, which we interpreted as strain-induced mixing of polymer chains. We assumed further that this affects an additional enthalpic contribution (the mixed polymer chains tend to phase separate again) which increases the restoring forces of the chains. Similar results were observed for block−graft copolymers with cylindrical and disordered lamella-like morphologies after high strains and long time relaxation, where a residual orientation of either elongated chains or domain fragments was found. At low strain in the neo-Hookean region, a simple approach of spherical domains without a decrease in long-range order was observed. We identified four essential features to improve the mechanical behavior of these thermoplastic elastomers: (i) the distribution of the applied stress to several branches along the PI backbone chain, (ii) an appropriate high M_w of the PI spacer to enable high extension rations, (iii) an appropriate contour length of the grafts to achieve small domains to which the grafts are effectively connected to, and (iv) a random grafting of the arms resulting in a multimodal network. In contrast, it was found that domain functionality (number of grafts connected to the domain) is less important to achieve improved mechanical properties. However, it is essential that these domains are highly deformable. Taking these molecular and morphological aspects into account, we can state further that while an increase of number of branch points mainly results in reduced hysteresis softening and increasing physical cross-link modulus, a random grafting additionally contributes to the chemical cross-link modulus.

AUTHOR INFORMATION

Corresponding Author

*E-mail: roland.weidisch@iwmh.fraunhofer.de. Tel: (+49)3455589430.

ACKNOWLEDGMENT

The authors thank for financial support of this work within the framework of the German Science Foundation (DFG) and Fraunhofer IWM Halle. A portion of this research at Oak Ridge National Laboratory's Center for Nanophase Materials Sciences was sponsored by the Scientific User Facilities Division, Office of Basic Energy Sciences, U.S. Department of Energy (enabled through User Project # 2003-028), and supported in part by the Division of Materials Science and Engineering, Office of Basic Energy Sciences, U.S. Department of Energy (DE- ACO5-00OR22725). Y. X. Duan thanks the support from Shang dong Province Science Fund (ZR2009AL011). We thank DESY for beamtime within the project II-20060086.

REFERENCES

(1) Gido, S. P.; Lee, C.; Pochan, D. J.; Mays, J. W.; Hadjichristidis, N. *Macromolecules* **1996**, *29*, 7022–7028.

(2) Xenidou, M.; Hadjichristidis, N. *Macromolecules* **1998**, *31*, 5690–5694.

(3) Uhrig, D.; Mays, J. W. *Macromolecules* **2002**, *35*, 7182–7190.

(4) Mays, J. W.; Uhrig, D.; Gido, S.; Zhu, Y.; Weidisch, R.; Iatrou, H.; Hadjichristidis, N.; Hong, K.; Beyer, F.; Lach, R.; Buschnakowski, M. *Macromol. Symp.* **2004**, *215*, 111–126. Uhrig, D.; Mays, J. *Polym. Chem.* **2011**, *2*, 69–76.

(5) Roos, A.; Creton, C. *Macromolecules* **2005**, *38*, 7807–7818.

(6) Staudinger, U.; Schlegel, R.; Weidisch, R.; Fritzsche, J.; Klüppel, M.; Heinrich, G.; Mays, J. W.; Uhrig, D.; Hadjichristidis, N. *Eur. Polym. J.* **2009**, *44*, 3790–3796.

(7) Schlegel, R.; Wilkin, D.; Duan, Y.; Weidisch, R.; Heinrich, G.; Uhrig, D.; Mays, J. W.; Iatrou, H.; Hadjichristidis, N. *Polymer* **2009**, *50*, 6297–6304.

(8) Duan, Y.; Rettler, E.; Schneider, K.; Schlegel, R.; Thunga, M.; Weidisch, R.; Siesler, H. W.; Stamm, M.; Mays, J. W.; Hadjichristidis, N. *Macromolecules* **2008**, *41*, 4565–4568.

(9) Duan, Y.; Thunga, M.; Schlegel, R.; Schneider, K.; Rettler, E.; Weidisch, R.; Siesler, H. W.; Stamm, M.; Mays, J. W.; Hadjichristidis, N. *Macromolecules* **2009**, *4*, 4155–4164.

(10) Sumpter, B. G.; Mays, J. W.; Noid, D. W.; Gido, S. P.; Weidisch, R. *Polym. News* **2004**, *29*, 302–310.

(11) Zhu, Y.; Burgaz, E.; Gido, S. P.; Staudinger, U.; Weidisch, R.; Uhrig, D.; Mays, J. W. *Macromolecules* **2006**, *3*, 4428–4436.

(12) Schneider, K.; Trabelski, S.; Zafeiropoulos, N. E.; Davies, R.; Riekel, C.; Stamm, M. *Macromol. Symp.* **2006**, *236*, 241–248.

(13) Rubinstein, M.; Panyukov, S. *Macromolecules* **2002**, *35*, 6670–6686.

(14) Klüppel, M. *Adv. Polym. Sci.* **2003**, *164*, 1–84.

(15) Langley, N. R.; Polmanteer, K. E. *J. Polym. Sci., Polym. Phys.* **1974**, *12*, 1023–1034.

(16) Klüppel, M.; Schramm, J. *Macromol. Theory Simul.* **2000**, *9*, 742–754.

(17) Kaliske, M.; Heinrich, G. *Rubber Chem. Technol.* **1999**, *72*, 602–632.

(18) Elías-Zúñiga, A. *Polymer* **2005**, *46*, 3496–3506.

(19) Zhu, Y.; Weidisch, R.; Gido, S. P.; Velis, G.; Hadjichristidis, N. *Macromolecules* **2002**, *35*, 5903–5909.

(20) Huang, Y.-Y.; Chen, H.-L.; Hashimoto, T. *Macromolecules* **2003**, *36*, 764–770.

(21) Milner, S. T. *Macromolecules* **1994**, *27*, 2333–2335.

(22) Beyer, F.; Gido, S. P.; Büschl, C.; Iatrou, H.; Uhrig, D.; Mays, J. W.; Chang, M. Y.; Garetz, B. A.; Balsara, N. P.; Tan, N. B.; Hadjichristidis, N. *Macromolecules* **2000**, *33*, 2039–2048.

(23) Mijović, J.; Sun, M.; Pejanović, S.; Mays, J. W. *Macromolecules* **2003**, *36*, 7640–7651.

(24) Thunga, M.; Schlegel, R.; Staudinger, U.; Duan, Y.; Weidisch, R.; Heinrich, G.; Mays, J. W.; Hadjichristidis, N. *Kautsch. Gummi Kunstst.* **2008**, *11*, 597–605.

(25) Matsen, M. W.; Tompsen, R. B. *J. Chem. Phys.* **1999**, *111*, 7139–7145.

(26) Ding, Y.; Kisliuk, A.; Sokolov, A. P. *Macromolecules* **2004**, *37*, 161–166.

(27) Morrison, F. A.; Winter, H. H. *Macromolecules* **1989**, *22*, 3533–3540.

(28) Schlegel, R.; Staudinger, U.; Thunga, M.; Weidisch, R.; Heinrich, G.; Uhrig, D.; Mays, J. W.; Iatrou, H.; Hadjichritidis, N. *Eur. Polym. J.* **2008**, *45*, 2902–2912.

(29) Mark, J. E. *Rubber Chem. Technol.* **1999**, *72*, 465–480.

(30) Stribeck, N. *X-ray Scattering of Soft Matter*; Springer: Berlin, 2007.

(31) Göritz, D. *Colloid Polym. Sci.* **1982**, *260*, 1993–197.

(32) Dlubek, G. Positron Annihilation Spectroscopy. In *Encyclopedia of Polymer Science and Technology*; Seidel, A., Hoboken, N. J., Eds.; John Wiley & Sons: New York, 2008.